Journal of Power Sources 189 (2009) 1167–1173

Contents lists available at ScienceDirect

Journal of Power Sources

journal homepage: www.elsevier.com/locate/jpowsour

Short communication

Electrochemical performance evaluation of polyaniline/lithium manganese nickel oxide composites synthesized using surfactant agents

Silmara Neves*, Sheila C. Canobre, Rafael S. Oliveira, Carla Polo Fonseca

Laboratório de Caracterização e Aplicação de Materiais - LCAM, Universidade São Francisco - Campus Itatiba, Itatiba 13251-900, SP, Brazil

ARTICLE INFO

Article history:
Received 27 October 2008
Received in revised form 10 January 2009
Accepted 12 January 2009
Available online 31 January 2009

Keywords:
Composite materials
Oxides
Polymers
Electrochemical properties
Surfactants
Polyaniline

ABSTRACT

The effect of adding a non-ionic surfactant to disperse oxide particles on the electrochemical performance of PAni/$LiMnNiO_4$ composites is evaluated by using cyclic voltammetry (CV), impedance measurements and constant-current charge/discharge cycling techniques. Three surfactants based on ethoxylated (EO) and propoxylated (PO) lauryl alcohols (3EO/6PO, L306; 4EO/5PO, L405; and 6EO/3PO, L603) were investigated. For comparative purposes, the oxide and polyaniline were prepared by sol–gel and chemical methods and were also investigated for their physical and electrochemical performances. By galvanostatic charge–discharge tests, the PAni/$LiMnNiO_4$ L306 composite showed a better electrochemical performance than each single component and other composites (PAni/$LiMnNiO_4$ L405 and PAni/$LiMnNiO_4$ L603). The electrical conductivity of this composite reached 21.7 S cm^{-1}, and an initial discharge capacity of 198 mAh g^{-1} was obtained. After 21 cycles, the retention capacity was 91%. These results indicate a synergistic effect among the materials in the composite.

Analytical techniques, such as scanning electron microscopy (SEM), X-ray diffraction spectroscopy (XRD) and inductively coupled plasma-atomic emission spectrometry (ICP-AES) were also used to characterize the composite materials.

1. Introduction

Today, the demand for rechargeable batteries with high energy densities and high voltages has rapidly increased due to the advancement and popularity of portable electronic devices. Among the possible new cathode materials for Li-ion batteries, $LiMn_2O_4$ spinel compounds, in which manganese atoms are partially substituted by nickel, copper, cobalt, chromium, titanium, or aluminum, have attracted much attention in recent years [1–5]. According to reports by Ohzuku and Makimura [6], a layered transition metal oxide such as $LiNi_{0.5}Mn_{0.5}O_2$ presents several advantages, mainly because it does not transform to the spinel structure during electrochemical cycling and it shows no sign of structural degradation due to multiphase reactions at higher voltages (>4.3 V), which are the major drawbacks associated with $LiMnO_2$ and $LiNiO_2$, respectively [7]. The lithium reinsertion is facilitated by $LiNi_{0.5}Mn_{0.5}O_2$, which exhibits dischargeable capacities of *ca.* 120 and 150 mAh g^{-1} at 2.8–4.3 and 2.8–4.6 V, respectively, with slight capacity fades. Furthermore, because the Mn content is higher and the Ni content is lower than in $LiNiO_2$, $LiNi_{0.5}Mn_{0.5}O_2$ is both cost-effective and less toxic, and an improved thermal safety is anticipated. It has also been shown that the $LiNi_{0.5}Mn_{0.5}O_4$ powder, calcinated at 950 °C, shows the best electrochemical performance with an initial discharge capacity of 139 mAh g^{-1} and 96% retention after 50 cycles [8].

However, further improvement is needed before the material is suitable for practical uses. To date, very little research on the electronic transport of doped manganese spinel has been performed. One point that is known is that its conductivity value is low (10^{-4} S cm^{-1}) [9].

Conductive polymers, such as polyaniline (PAni), conduct electricity mainly by the movement of charge carriers known as polarons and bipolarons, generated when the polymer is slightly oxidized [10]. These materials can be used as cathodes in secondary batteries because they can be reversibly oxidized and reduced, and thus they can be switched reversibly from an insulating to a conducting state. Doped polyanilines have also been satisfactorily combined with inorganic redox oxides, producing systems suitable for electrochemical Li intercalation. Kanatzidis et al. [11] described the intercalative polymerization of aniline in a V_2O_5 xerogel, yielding PAni nanocomposites of good electrical conductivity, and Nazar and co-workers [12,13] demonstrated the feasibility of using these materials for reversible electrochemical lithium insertion. The $[PAni]_{0.3}V_2O_5$ presented a specific capacity of 181 mAh g^{-1} and an energy density of 507 Wh kg^{-1} higher than those obtained for pure oxide (120 mAh g^{-1} and 384 Wh kg^{-1}) due to the synergistic effect resultant from the contact between PAni and V_2O_5 [14]. In

* Corresponding author. Tel.: +55 11 4534 8071; fax: +55 11 4524 1933.
E-mail address: silmara.neves@saofrancisco.edu.br (S. Neves).

0378-7753/$ – see front matter © 2009 Elsevier B.V. All rights reserved.
doi:10.1016/j.jpowsour.2009.01.061

addition to these materials, there are also those called microcomposites, i.e., polymeric materials combined at the micrometer scale, or even nanocomposites, taking into account the micrometer or nanometer scale size of the oxide particles involved [15–18]. Thus, the combination of these two types of materials (mixed oxides and conducting polymers) generates a class of mixed conduction composites with unique properties and relatively simple synthesizing procedures.

The classical methods for synthesizing spinel $LiMn_2O_4$ materials are via solid-state [19] or sol–gel methods [20]. However, both methodologies agglomerate nanoparticles, making the synthesis of nanocomposites difficult.

In this context, we have been exploring the idea of using several surfactants to disperse the $LiMn_{2-x}Ni_xO_4$ particles before their use as a template for the synthesis of a conducting polymer (polyaniline). The goal of this procedure is to promote better coverage of the oxide nanoparticles in order to improve their electrochemical performance for their application as cathodes in secondary batteries. The effects of the choice of surfactant on the resulting nanocomposites were investigated.

2. Experimental

2.1. Synthesis of $LiMn_{2-}Ni_xO_4$

A typical sol–gel synthesis of $LiMn_{2-x}Ni_xO_4$ with citric acid as a chelating agent was performed in the following way: stoichiometric amounts of lithium acetate, nickel nitrate and manganese acetate (Aldrich) were dissolved in citric acid and an ethylene glycol (1:4, v/v) solution. Upon stirring, the mixture turned into a viscous sol, which was then heated at 160 °C, resulting in the formation of a gel precursor upon the evaporation of solvents. A subsequent heat treatment was carried out at 250–900 °C in air with isotherms for 30 min at 250, 500 and 900 °C, followed by a natural cooling step to obtain $LiMn_{2-x}Ni_xO_4$ powders.

2.2. Synthesis of PAni

Polyaniline was synthesized chemically as emeraldine salt (ES) by oxidative polymerization of a distilled monomer (12.6 mmol L^{-1}) in a solution containing 1 mol L^{-1} HCl, 3 mol L^{-1} NaCl and 6.25 mmol L^{-1} citric acid at −10 °C. Another solution containing 1 mol L^{-1} HCl, 3 mol L^{-1} NaCl and 0.03 mol L^{-1} of ammonium persulfate $(NH_4)_2S_2O_8$, was added to the aniline solution over a period of 3 h with vigorous stirring. The precipitate was collected by filtration and then washed with 1 mol L^{-1} HCl, resulting in the conductive state of the polyaniline (emeraldine). The dark powder was dried under a dynamic vacuum for 48 h.

2.3. Synthesis of PAni/$LiMn_{2-x}Ni_xO_4$

Firstly, 150 mg of the $LiMn_{2-x}Ni_xO_4$ powders were dispersed for 10 min in an ultra-sonic bath using 1 mL of a surfactant agent in a solution containing 1 mol L^{-1} HCl and 3 mol L^{-1} NaCl. Three commercial non-ionic surfactants were investigated, viz. L306, L405 and L603, which are part of the range trade named Alkomol® (OXITENO Inc., Brazil). They were all ethoxylated and propoxylated alcohols with average molecular weights of 675, 661 and 646 g mol^{-1}, respectively. Their structures, which consist of a hydrophobic backbone with a hydrophilic group attached, may be represented as

$$RO(CH_2CH_2O)_n(CH_2CH_2CH_2O)_mH$$

where R is the grease chain of the alcohol, and n and m are the average mole numbers of ethylene oxide and propylene oxide, respectively. Then, the surfactants used are EO/PO lauryl alcohols with the following proportions: 3EO/6PO (L306), 4EO/5PO (L405) and 6EO/3PO (L603). The ethylene oxide unit was water soluble while the propene oxide was not; their combination in single segments yields a surfactant with amphiphilic characteristics, which are regarded as the best steric stabilizers [21].

To coat the dispersed $LiMn_{2-x}Ni_xO_4$ powder with polyaniline, 12.6 mmol L^{-1} of aniline was introduced, and the solution was cooled at −10 °C. Then, the oxidant solution (0.03 mol L^{-1} ammonium persulfate in 1 mol L^{-1} HCl and 3 mol L^{-1} NaCl) was added over a period of 3 h with vigorous mechanical stirring. As described in Section 2.2, the precipitate was collected by filtration and washed with 1 mol L^{-1} HCl. The dark powder was also dried under a dynamic vacuum for 48 h.

2.4. Preparation of cathode films

Several cathode electrodes were obtained by mixing each PAni/$LiMn_{2-x}Ni_xO_4$ composite with polyvinylidene fluoride (PVDF; 8 wt.%; Fluka, MW = 10^5 g mol^{-1}) in N,N-dimethyl acetamide. The films were obtained by spin-coating (5000 rpm, 5 s) each mixture onto platinum plates. Prior to use, the electrodes were dried at 60 °C. These electrodes were prepared to evaluate the performance of the composites as a function of the kind of surfactant used in the synthesis.

2.5. Characterization

The conductivity was measured by a co-linear four-point technique on pellets compressed at 2 MPa. The diameter of the pellets was typically 1.00 cm, and the thickness was 0.07 cm. Electrical measurements were performed in a conditioned laboratory at 20 °C using four probe tips (Cascade Microtech C4S-54; distance between probes = 0.127 cm), an ampere meter, a DC current source, and a voltmeter (Minipa). All data were used to calculate the conductivity values of each sample. Proper correction factors were employed based on the sizes and shapes of the specimens.

The powders were also characterized by X-ray diffraction (XRD) using a Shimadzu model XRD 7000, with Cu Kα radiation (40 kV–30 mA) at 2° min^{-1}. The counting time was 10 s for the entire spectrum, $2^\circ \leq 2\theta \leq 90^\circ$. The composition of the mixed oxide was determined by an inductively coupled plasma-atomic emission spectrometer (ICP-AES, Perkin Elmer 3000 DV) after dissolving the given powder sample in HNO_3.

Scanning electron microscopy was done with a JEOL model JSM-5900LV–LNLS/Campinas microscope after coating the sample powders with gold by sputtering using a *sputter coater*, SCD model 50.

Electrochemical tests were done in a liquid electrolyte at room temperature using 1 mol L^{-1} $LiClO_4$ in a 1:1 mixture of ethylene carbonate (EC) and dimethylene carbonate (DMC). The electrodes were cycled in cells with thick lithium foils as the negative and reference electrodes. The electrochemical cells containing different cathodes were characterized using cyclic voltammetry, in the potential range from 2.9 to 4.4 V at 1 mV s^{-1}, and charge/discharge tests, applying current densities of ±10 and ±20 μA cm^{-2} depending on each sample. The mass of the composite was used in the capacity calculation. All electrochemical experiments were performed in an argon-filled dry box using an AUTOLAB—PGSTAT30 FRA.

3. Results and discussion

3.1. Material characterization

In this study, the Ni content in the oxide samples, as measured by ICP analysis, was about $x = 1.0$ in the $LiMn_{2-x}Ni_xO_4$ form. The

Table 1
Elemental composition of $LiMn_{2-x}Ni_xO_4$ sample, obtained by ICP analysis.

Nominal composition	$LiMn_{2-x}Ni_xO_4$
Experimental composition (wt.%)	
Li	4.27 ± 0.07
Mn	28.4 ± 3.1
Ni	31.3 ± 2.5

values obtained by the elemental analysis are shown in Table 1. In general, Mn substitution with some metal ions decreases the initial discharge capacity and improves the electrochemical cyclability of spinel $LiMn_2O_4$ by increasing the average Mn valence [22].

To find out the crystallinity of the oxide, conductive polymer and composites synthesized in the presence of different surfactant agents, XRD analysis was performed, and the resultant XRD pattern is shown in Fig. 1. In the profile obtained for $LiMnNiO_4$ (Fig. 1a), the α-$NaFeO_2$ layered rhombohedral structure with an R3-*m* space group is well established, in agreement with reports in the literature [7,23–27]. The higher intensity ratio of the (0 0 3) and (1 0 4) diffraction peaks, as well as the clearer splitting of the (0 0 6)/(1 0 2) and (1 0 8)/(1 1 0) diffraction peaks, confirmed the layered nature of the material [28,29]. The average crystal size (calculated from the Scherrer equation [30]) and the ratios of the integrated intensity of the (0 0 3) peak to that of the (1 0 4) peak, i.e., (*R* 0 0 3/1 0 4), were 23.3 and 1.16 nm, respectively. The *R*(0 0 3)/(1 0 4) was usually taken as an approximate measure of the amount of ion mixing in the α-$NaFeO_2$-type structured material [31,32]. Higher values of *R*(0 0 3)/(1 0 4), as obtained, were desirable, and they corresponded to an ideal structure in which fewer Li ions would locate in the transition metal site.

The PAni chain produced under acidic conditions has fewer structural defects (e.g., nonpara linkage in PAni-chains), which results in the fractions of crystalline phase observed by DRX [33], seen in Fig. 1. Two peaks centered at $2\theta = 20^\circ$ and 25° were verified in the X-ray scattering patterns of polyaniline (emeraldine salt-ES) and all the composite samples. The peak centered at $2\theta = 20^\circ$ (1 0 0 face) is ascribed to a periodicity parallel to the polymer chain, while the peak at $2\theta = 25^\circ$ (1 1 0 face) is due to the periodicity perpendicular to the polymer chain [34]. The peak at $2\theta = 20^\circ$ also represents the characteristic distance between the planes of benzene rings in adjacent chains or the close contact interchain distance [35]. For ES and composite L306 samples, the peak at $2\theta = 25^\circ$ is stronger than that at $2\theta = 20^\circ$, which is similar to that seen for highly doped

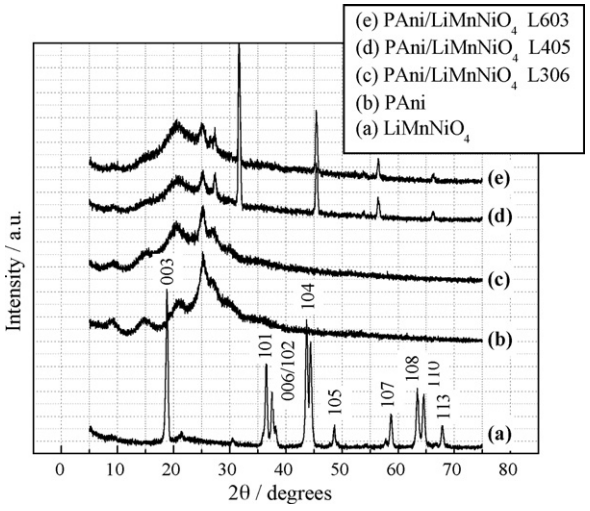

Fig. 1. XRD patterns of the $LiMnNiO_4$, PAni and composites synthesized with different surfactant agents. Counting time of 10 s in the range of the $5^\circ \leq 2\theta \leq 75^\circ$.

polyaniline [36,37]. However, for the composites obtained with the surfactants L405 and L603, the peak at $2\theta = 25^\circ$ has the same magnitude as that at $2\theta = 20^\circ$. It was found that an increase in the concentration of ethoxylated groups in the surfactant agents causes an increase of the periodicity parallel to the polyaniline chains. This observation can be rationalized in terms of physical bonds (hydrogen bonds or van der Waals bonds) between the EO/PO segment interchains, which result in the crystalline phases ($2\theta = 32^\circ$, 45°, 57° and 66°) responsible for inducing the orientation of PAni chains.

The main diffraction peaks of the oxides disappeared in all the composites, and the pattern characteristic of PAni predominated. This may be attributed to the interaction between the PAni and oxide, which is improved by the presence of surfactants. A similar behavior was observed by Singla et al. [38] in composites constituted by Mn_3O_4 and PAni doped with different acids, where the interaction between the oxide and counter acid anion was responsible for the disappearance in the XRD diffraction pattern of Mn_3O_4.

Fig. 2 shows typical SEM micrographs recorded for all the materials studied. It can be seen from Fig. 2a and b that the as-prepared $LiMnNiO_4$ powder shows a narrow particle size distribution, but conglomeration among the particles is clearly observed. The particles are about 0.5–4 μm in size. The discrepancy in the particle sizes obtained from SEM and XRD analyses originates from the presence of impurities and the tendency of the crystallites to agglomerate into secondary particles. It also suggests a greater tendency toward agglomeration in the sol–gel material. Fig. 2c and d shows the larger agglomerates of polyaniline, which form some slabs with superficial crystalline structures, in agreement with the XRD pattern. The distribution of the polyaniline in the composites was evaluated in Fig. 2e–j. The synthesis of the composites resulted in agglomerates with irregular particles formed by small oxide crystallites stuck together with polymer plates. The SEM images show that, independent of the kind of surfactant, the oxide surface in contact with the reaction mixture used for the polymerization of aniline becomes coated with PAni particles. It is assumed that aniline oligomers are produced first [39]. Because of their reduced solubility, they adsorb at the available interfaces. The adsorbed species start the growth of PAni chains, which is why polymerization at an interface is preferred for the corresponding process in the whole volume of a reaction mixture [40,41]. The polymerization of aniline is auto-accelerated [42]; i.e., PAni formation preferentially occurs at the spots where some PAni has already been produced. This leads to a proliferation of the PAni film nucleated at the interface of the $LiMnNiO_4$-surfactant, resulting in an effective cover. All the composites presented particle agglomeration, as in Fig. 2e–j. The presence of aromatic rings in the coating molecule may aid the aggregation of the particles, possibly due to an attractive interaction between the π-systems of molecules on neighboring particles, which would have significant strength when summed over the number of molecules adsorbed on a typical particle surface. A similar effect is seen in the molecular crystals of aromatic compounds, where the crystal structure is maintained by the stacking interactions of adjacent molecules [43]. The presence of some crystals can be observed in the micrographs recorded for the composites with the surfactants L405 and L603, in agreement with the DRX results (Fig. 1).

The conductivity of all the samples was determined by the colinear four-probe technique. The values are presented in Table 2. The polyaniline doped with HCl has a high crystallinity and electrical conductivity, concurring with similar results that have been reported in the literature [44]. The measured value of the electrical conductivity of the oxide was on the order of 10^{-5} S cm^{-1} at room temperature, and this value falls within the semiconductor range (10^{-10} to 10^{-4} S cm^{-1}). The conductivity of the PAni/$LiMnNiO_4$ L306 composite was four times greater than that of neat PAni and other composites, which can be ascribed to the formation of more ordered

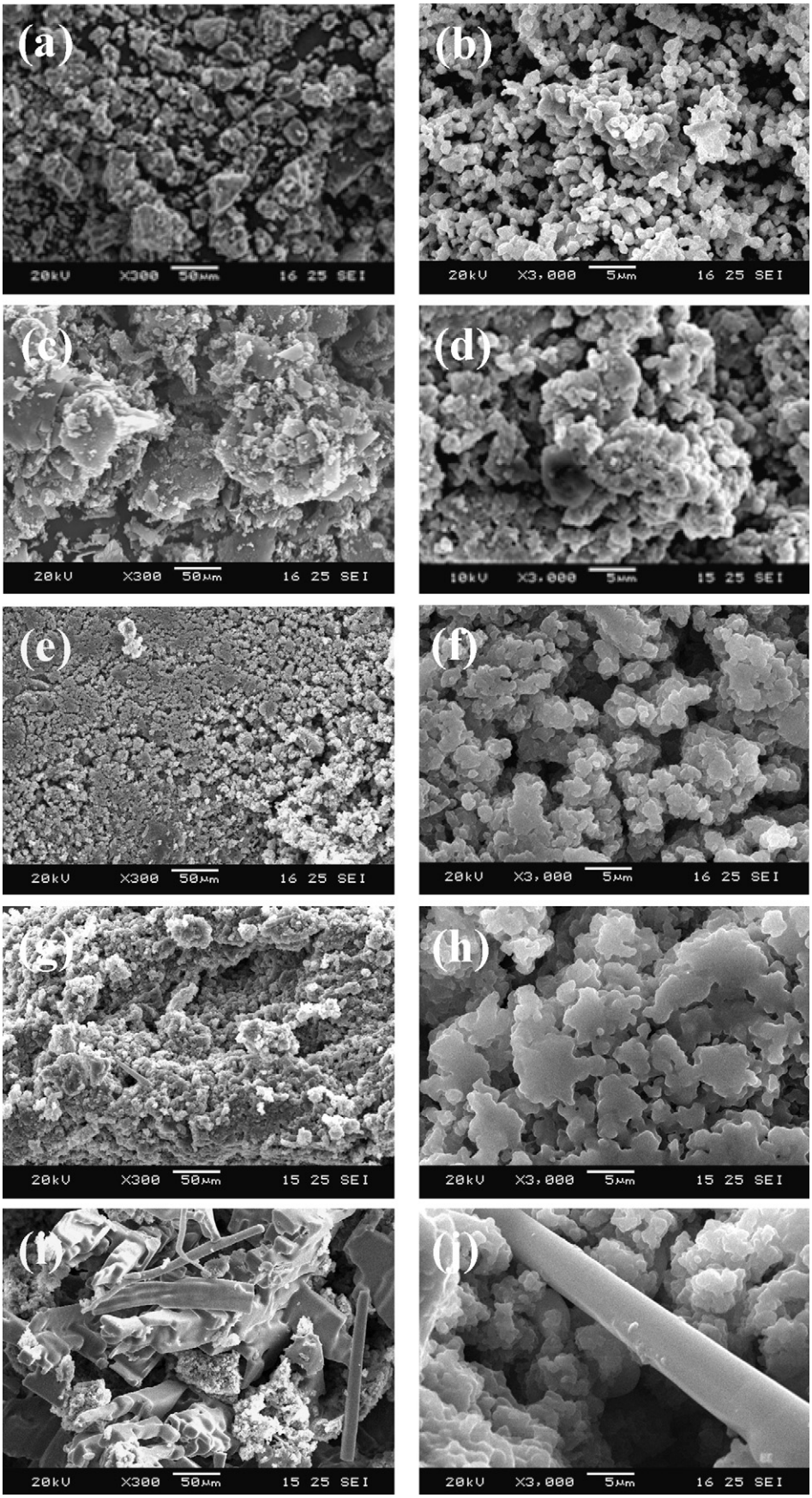

Fig. 2. SEM images of $LiMnNiO_4$ (a and b), PAni (c and d) and PAni/$LiMnNiO_4$ synthesized with surfactant L306 (e–f), L405 (g and h), L603 (i and j). Magnification: 300 and 3000×.

Table 2
Four-probe conductivity values of oxide, polyaniline and PAni/$LiMnNiO_4$ composites.

Materials	σ/S cm^{-2}
PAni	5.4
$LiMnNiO_4$	$<10^{-5}$
PAni/$LiMnNiO_4$ L306	21.7
PAni/$LiMnNiO_4$ L405	6.5
PAni/$LiMnNiO_4$ L603	8.2

Table 3
Impedance parameters determined from Bode-type diagrams.

Sample	Z_T (Ω cm^2)	R_e (kΩ cm^2)	D (cm^2 s^{-1})
$LiMnNiO_4$	62,089	56.5	2.4×10^{-10}
PAni	281	46.8	8.37×10^{-6}
PAni/$LiMnNiO_4$ L306	4,812	80.0	1.8×10^{-7}
PAni/$LiMnNiO_4$ L405	5,147	91.4	4.4×10^{-9}
PAni/$LiMnNiO_4$ L603	2,658	53.8	2.4×10^{-8}

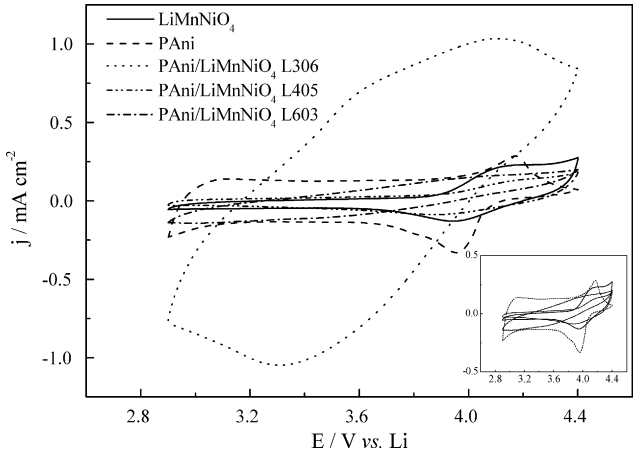

Fig. 3. Steady state cyclic voltammograms obtained using 1 mol L^{-1} $LiClO_4$ in EC–DMC as electrolyte solution, at 1 mV s^{-1}. Inset shows the magnification of lower current density range.

PAni chains, induced by the presence of surfactant L306, that favor the interaction between the π-conjugated structures of the quinoid.

3.2. Electrochemical performance

Typical CV obtained in the present case for composites of PAni/$LiMnNiO_4$ and individual components are depicted in Fig. 3. The current responses are presented as normalized with the weight of the sample films. The cycle performance was not investigated over 4.4 V to avoid polyaniline degradation. $LiMnNiO_4$ showed major oxidation and reduction peaks at around 4.1 and 3.9 V, respectively, corresponding to the lithium deintercalation and reintercalation processes (Fig. 3b). These observed peaks could be assigned to an Mn^{3+}/Mn^{4+} electrochemical process [45].

Fig. 3 also shows a couple of poorly defined redox peaks for polyaniline centered at 4.2/4.0 V. However, no obvious redox peaks were observed in the voltammetries of all the composites, indicating that capacitive behavior is predominant. Significant increases in the current density were observed for the PAni/$LiMnNiO_4$ L306, which appears to be due to a better interaction between the conductive polymer and the oxide that was promoted by the surfactant with a lower concentration of EO groups and, therefore, a lower crystallinity. It seems that the crystalline and dense structures of the composites L405 and L603 retard the ionic motion in the electrodes, resulting in a decrease in the electroactivity.

Impedance analysis of the $LiMnNiO_4$, PAni and PAni/$LiMnNiO_4$ composite films at OCP is shown in Fig. 4 as Bode-type diagrams. The total impedance of the $LiNiMnO_4$ film (Z_T) determined at a lower frequency range was higher than that of the PAni/$LiMnNiO_4$ composite films, as presented in Table 3. This difference is attributed to the presence of PAni in the composites, which increased the electronic conductivity and also acted as an electroactive material.

Despite the fact that all the films were characterized in the same electrolyte solution, the values determined for the electrolyte resistance (R_e) at a high frequency range changed as a function of the surfactant present in the composite, as in Fig. 4a and Table 3. The hypothesis to justify this behavior is that, during composite synthesis, the molecules of aniline become progressively incorporated into the interior of the oxide/surfactant aggregates and that, when an oxidant agent is added to the recipient, the oxidative polymerization begins to take place, both in the interior and exterior of these aggregates. The conducting polymer chains are trapped inside the surfactant aggregates, with parallel and/or perpendicular structures. The surfactants used in the composites' syntheses are formed by EO/PO chains, which can participate in the ion transport through lithium-polymer chain complexes. It is important to consider that the materials most studied as polymer electrolytes are precisely based on poly(ethylene oxide) (PEO) and poly(propylene oxide) (PPO), both of which contain inorganic salt dissolved in their matrices [46,47]. Therefore, we believe that the electrolyte resistance variation is due to the additional participation of the surfactant as an electrolyte.

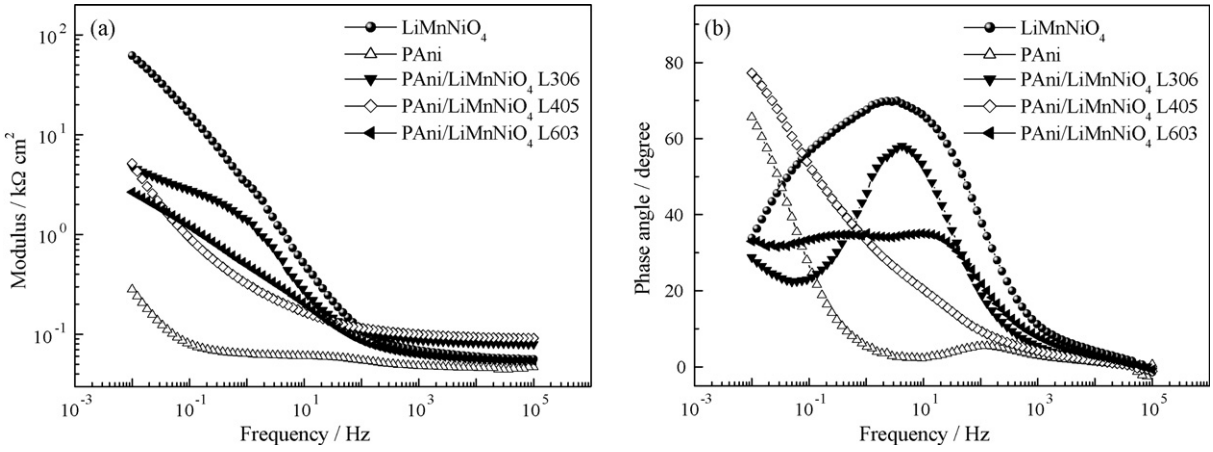

Fig. 4. Frequency dependence of the impedance of the modulus (a) and phase (b) parts of PAni/$LiMnNiO_4$ composite films and individual components obtained at OCP (3.3 V *vs.* Li) in EC–DMC/1.0 mol L^{-1} $LiClO_4$.

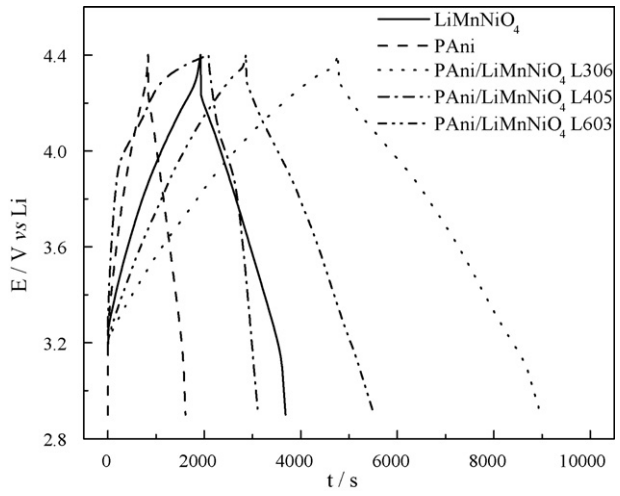

Fig. 5. Initial charge and discharge curves where $j = \pm 10\,mA\,cm^{-2}$ for PAni, $LiMnNiO_4$, composites L306 and 603 samples and $\pm 20\,mA\,cm^{-2}$ for composite L405. The mass used of each sample was 50 mg, approximately.

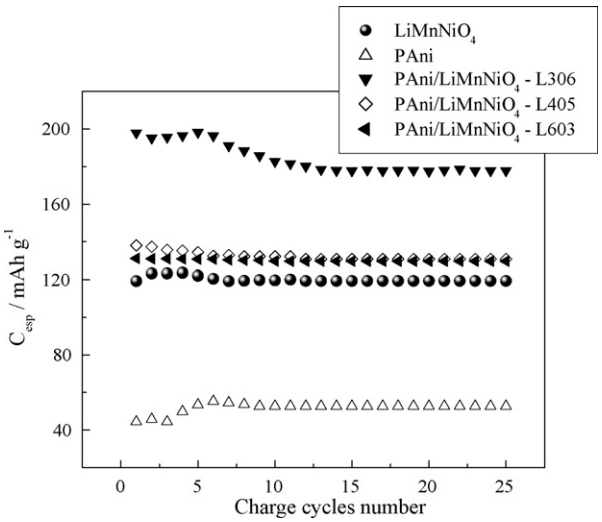

Fig. 6. Variation of the capacity delivered by the cells as a function of the number of cycles.

The inclined line in the low-frequency range was attributed to the 'Warburg impedance' associated with lithium diffusion through the composite electrode [48]. The chemical diffusion coefficient (D) can be estimated through the plot's frequency dependency of the imaginary part (Fig. 4b) using $\omega = 2D/h^2$, where ω is the transition angular velocity and h is the film thickness (13.25 μm). The values of the diffusion coefficients presented in Table 3 for $LiMnNiO_4$ and PAni are in agreement with results reported in the literature [49–51]. With respect to composites, the L306 presented a diffusion coefficient higher than the other composites, probably related to the more perpendicular configuration of the polyaniline chains indicated in the XRD analysis (Fig. 1), which facilitates the process of ion diffusion in the bulk of the material. Another fact that can be considered is the presence of crystalline phases in the composites L405 and L603, which inhibits access of the electrolyte solution to oxide particles.

Typical initial charge–discharge profiles of Li/$LiMnNiO_4$ cells are presented in Fig. 5. To further investigate the effect of the surfactant on the long-term stability of the Li-ion cell, the cells containing composite films as cathodes were charged to 4.4 V after every 25 cycles, and the relationship between the specific capacitance and the cycle number are plotted in Fig. 6. The electrochemical performances are presented in Table 4.

The $LiMnNiO_4$ sample shows an initial discharge capacity of 122 mAh g^{-1} and good cycle behavior, as it retained a discharge capacity of 119 mAh g^{-1} after 25 cycles, which corresponds to 98% retention capacity. This may be due to its lamelar structure, where lithium ions can deintercalate/intercalate in the layered space during the charge/discharge processes. This result is promising mainly because the charge/discharge cycling has been performed between the cut-off voltages of 2.8 and 4.4 V [52,53]. The specific capacity value determined for polyaniline was initially 55 mAh g^{-1}, which is in agreement with the results reported in the literature [54] for PAni obtained with a similar polymerization method, solvent and electrolyte salt. After 25 cycles, the discharge capacity slowly reduces but still retains 96% of the initial value.

Under the same conditions, the discharge capacity of the PAni/$LiMnNiO_4$ L306 composite at the 25th cycle was 181 mAh g^{-1}; this was a very good result even when a retention capacity of 91% is considered. The advantages of synthesizing the composites using the surfactants L405 and L603 were not so evident; the specific capacity values determined after 25 cycles were closer than those obtained from only oxide, at 131, 130 and 119 mAh g^{-1}, respectively.

This good electrochemical performance of mainly the PAni/$LiMnNiO_4$ L306 composite can be attributed to the effective interaction between the conductive shell of PAni and the core of $LiMnNiO_4$ L306, and/or due to the increase of the mass fraction of electrochemically active oxide exposed to an electrolyte as promoted by the surfactant L306. However, to elucidate the mechanism of the interaction between these possibilities requires further studies. Comparing the cycling performance of all the tested materials (Table 4), it is evident that the composite PAni/$LiMnNiO_4$ L306 is a promising alternative to traditional materials used, such as for the cathodes in lithium ion batteries.

Table 4
Electrochemical performance of materials.

Sample	5th discharge capacity (mAh g^{-1})	25th discharge capacity (mAh g^{-1})	Retention capacity[a] (%)
$LiMnNiO_4$	122	119	98
PAni	55	53	96
PAni/$LiMnNiO_4$ L306	198	181	91
PAni/$LiMnNiO_4$ L405	134	131	98
PAni/$LiMnNiO_4$ L603	131	130	99

[a] Retention capacity = (25th discharge capacity/5th discharge capacity) × 100%.

4. Conclusions

Composites of PAni and $LiMnNiO_4$ can be obtained by the oxidative polymerization of aniline in a medium containing oxide. These composites present a class of materials containing an inorganic host that was encapsulated or uniformly coated with conducting polymers due to the presence of non-ionic surfactants based on EO/PO lauryl alcohols.

Powder X-ray diffraction data showed that an ideal structure was obtained for $LiMnNiO_4$ in which fewer Li ions were located in the transition metal site. DRX and SEM confirmed the effective cover of the oxide/surfactant particles by polyaniline. The composite PAni/$LiMnNiO_4$ L306 showed the best electrochemical performance, with an initial capacity of 198 mAh g^{-1}; after 25 cycles, the retention capacity was 91%. The results showed coherence and indicated a synergistic effect among the constituents, which validates the strategy of designing high-capacity electrodes using integrated 'composite' structures.

Acknowledgements

The authors thank the LMF and LME/LNLS—National Synchrotron Light Laboratory, Campinas, SP, Brazil for technical support. This work was supported by FAPESP (grants 06/50967-1, 05/54578-7 and 07/54467-6), CNPq (grant 304386/2005-7) and the Universidade São Francisco.

References

[1] E. Machefaux, A. Verbaere, D. Guyomard, J. Power Sources 165 (2007) 625.
[2] Y.-P. Fu, Y.-H. Su, S.-H. Wu, C.-H. Lin, J. Alloys Compd. 426 (2006) 228.
[3] L. Pascual, M.L. Pérez-Revenga, R.M. Rojas, J.M. Rojo, J.M. Amarilla, Electrochim. Acta 51 (2006) 3193.
[4] H.M. Wu, J.P. Tu, Y.F. Yuan, J.Y. Xiang, X.T. Chen, X.B. Zhao, G.S. Cao, J. Electroanal. Chem. 608 (2007) 8.
[5] M.J. Iqbal, S. Zahoor, J. Power Sources 165 (2007) 393.
[6] T. Ohzuku, Y. Makimura, Chem. Lett. 30 (2001) 744.
[7] S.-H. Kang, K. Amine, J. Power Sources 119–121 (2003) 150.
[8] H.Y. Xu, S. Xie, N. Ding, B.L. Liu, Y. Shang, C.H. Chen, Electrochim. Acta 51 (2006) 4352.
[9] J. Marzec, K. Swierczek, J. Przewoznik, J. Molenda, D.R. Simon, E.M. Kelder, J. Schoonman, Solid State Ionics 146 (2002) 225.
[10] D.C. Trivedi, Handbook of Organic Conductive Molecules and Polymers, vol. 2, John Wiley & Sons, Chichester, 1997.
[11] M.G. Kanatzidis, C.-G. Wu, H.O. Marcy, C.R. Kannewurf, J. Am. Chem. Soc. 111 (1989) 4139.
[12] F. Leroux, B.E. Koene, L.F. Nazar, J. Electrochem. Soc. 143 (1996) L181.
[13] F. Leroux, G. Goward, W.P. Power, L.F. Nazar, J. Electrochem. Soc. 144 (1997) 3886.
[14] F. Huguenin, R.M. Torresi, Quim. Nova 27 (2004) 393.
[15] S. Maeda, S.P. Armes, J. Colloids Interf. Sci. 159 (1993) 257.
[16] R.F. Farias, J.M. Souza, J.V. Melo, C. Airoldi, J. Colloids Interf. Sci. 212 (1999) 123.
[17] H. Yoneyama, N. Takahashi, S. Kuwabata, J. Chem. Soc. Chem. Commun. (1992) 716.
[18] H. Yoneyama, A. Kishimoto, S. Kuwabata, J. Chem. Soc. Chem. Commun. (1991) 986.
[19] G. Li, A. Yamada, Y. Fukishima, K. Yamaura, T. Saito, T. Endo, H. Azuma, K. Sekai, Y. Nishi, Solid State Ionics 130 (2000) 221.
[20] S.W. Lee, S.Y. An, I.B. Shin, C.S. Kim (Eds.), Adv. Nanomaterials Nanodevices, 2002, p. 801.
[21] D.H. Napper, Polymeric Stabilization of Colloidal Dispersions, Academic Press, New York, 1983.
[22] W.T. Jeong, J.H. Joo, K.S. Lee, J. Power Sources 119–121 (2003) 690.
[23] E. Zhecheva, R. Stoyanova, Solid State Ionics 66 (1993) 143.
[24] N.J. Dudney, J.B. Bates, R.A. Zuhr, S. Young, J.D. Robertson, H.P. Jun, S.A. Hackney, J. Electrochem. Soc. 147 (1999) 2455.
[25] Y.W. Tsai, R. Santhanam, B.J. Hwang, S.K. Hu, H.S. Sheu, J. Power Sources 119–121 (2003) 701.
[26] D. Caurant, N. Baffier, B. Garcia, J.P. Pereira-Ramos, Solid State Ionics 91 (1996) 45.
[27] L. Hernán, J. Marales, L. Sánchez, J. Santos, J. Electrochem. Soc. 144 (1997) 1704.
[28] B.J. Hwang, R. Santhanam, C.H. Chen, J. Power Sources 114 (2003) 244.
[29] P. Periasamy, H.S. Kim, S.H. Na, S.I. Moon, J.C. Lee, J. Power Sources 132 (2004) 213.
[30] P. Scherrer, Nachr Ges. Wiss. Gottingen (1918) 98.
[31] G.T.K. Fey, J.G. Chen, V. Subramanian, T. Osaka, J. Power Sources 384 (2002) 112.
[32] J.M. Paulsen, C.L. Thomas, J.R. Dahn, J. Electrochem. Solid-State Lett. 147 (2000) 861.
[33] J. Stejskl, A. Riede, D. Hlabanta, J. Prokes, M. Helmstedt, P. Holler, Synth. Met. 96 (1998) 51.
[34] M.E. Jozefowicz, R. Laversanne, H.H.S. Javadi, A.J. Epstein, J.P. Pouget, X. Tang, A.G. MacDiarmid, Phys. Rev. B 39 (1989) 12958.
[35] Y.B. Moon, Y. Cao, P. Smith, A.J. Heeger, Polym. Commun. 30 (1989) 196.
[36] J.P. Pouget, M.E. Jozefowicz, A.J. Epstein, X. Tang, A.G. MacDiarmid, Macromolecules 24 (1991) 779.
[37] T.-M. Wu, Y.-W. Lin, C.-S. Liao, Carbon 43 (2005) 734.
[38] M.L. Singla, S. Awasthi, A. Srivastava, D.V.S. Jain, Sens. Actuators A: Phys. 136 (2007) 604.
[39] I. Sapurina, A. Riede, J. Stejskal, Synth. Met. 123 (2001) 503.
[40] M. Trchová, I. Sedenková, J. Stejskal, Synth. Met. 154 (2005) 1.
[41] S. Fedorova, J. Stejskal, Langmuir 18 (2002) 5630.
[42] K. Tzou, R.V. Gregory, Synth. Met. 47 (1992) 267.
[43] D.M. Donaldson, J.M. Robertson, J.G. White, Proc. R. Soc. Lond. A Mat. 220 (1953) 311.
[44] J.P. Pouget, C.H. Hsu, A.G. MacDiarmid, A.J. Epstein, Synth. Met. 69 (1995) 119.
[45] Y. Shin, A. Manthiram, Electrochim. Acta 48 (2003) 3583.
[46] M.B. Armand, J.M. Chabagno, M. Duclot, in: P. Vashista, J.M. Mundy, G.K. Sherroy (Eds.), Fast-ion Transport in Solids, North-Holland, Amsterdam, 1979.
[47] J.Y. Song, Y.Y. Wang, C.C. Wan, J. Power Sources 77 (1999) 183.
[48] Y.M. Choi, S.I. Pyun, Solid State Ionics 99 (1997) 173.
[49] E. Deiss, D. Haringer, P. Novak, O. Haas, Electrochim. Acta 46 (2001) 4185.
[50] E. Deiss, Electrochim. Acta 50 (2005) 2927.
[51] M.A. Careem, Y. Velmurugu, S. Skaarup, K. West, J. Power Sources 159 (2006) 210.
[52] Y. Gao, K. Myrtle, M. Zhang, J.N. Reimers, J.R. Dahn, Phys. Rev. B 54 (1996) 16679.
[53] K. Kanamura, W. Hoshikawa, Solid State Ionics 177 (2006) 113.
[54] P. Novák, K. Muller, K.S.V. Santhanam, O. Haas, Chem. Rev. 97 (1997) 207.